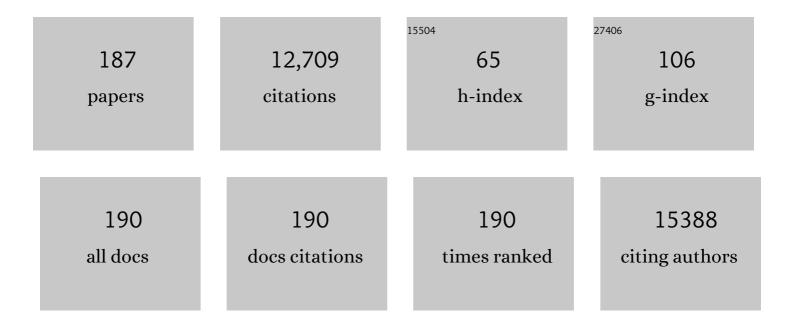
Tao Chen

List of Publications by Year in descending order

Source: https://exaly.com/author-pdf/4063562/publications.pdf Version: 2024-02-01



#	Article	IF	CITATIONS
1	Oriented Organization of Poly(3â€Hexylthiophene) for Efficient and Stable Antimony Sulfide Solar Cells. Energy and Environmental Materials, 2023, 6, .	12.8	2
2	Recent progress and perspectives on Sb2Se3-based photocathodes for solar hydrogen production via photoelectrochemical water splitting. Journal of Energy Chemistry, 2022, 67, 508-523.	12.9	85
3	Regulating Energy Band Alignment via Alkaline Metal Fluoride Assisted Solution Postâ€Treatment Enabling Sb ₂ (S,Se) ₃ Solar Cells with 10.7% Efficiency. Advanced Energy Materials, 2022, 12, .	19.5	93
4	9.6%-Efficient all-inorganic Sb ₂ (S,Se) ₃ solar cells with a MnS hole-transporting layer. Journal of Materials Chemistry A, 2022, 10, 2835-2841.	10.3	19
5	Organic Chloride Salt Interfacial Modified Crystallization for Efficient Antimony Selenosulfide Solar Cells. ACS Applied Materials & Interfaces, 2022, 14, 4276-4284.	8.0	16
6	Distinctive Deepâ€Level Defects in Nonâ€Stoichiometric Sb ₂ Se ₃ Photovoltaic Materials. Advanced Science, 2022, 9, e2105268.	11.2	34
7	Tuning the Interaction between Ruthenium Single Atoms and the Second Coordination Sphere for Efficient Nitrogen Photofixation. Advanced Functional Materials, 2022, 32, .	14.9	22
8	Dopant-free hole-transporting materials for stable Sb ₂ (S,Se) ₃ solar cells. Chemical Communications, 2022, 58, 4787-4790.	4.1	15
9	Tuning the Interaction between Ruthenium Single Atoms and the Second Coordination Sphere for Efficient Nitrogen Photofixation (Adv. Funct. Mater. 12/2022). Advanced Functional Materials, 2022, 32, .	14.9	0
10	An n–n type heterojunction enabling highly efficient carrier separation in inorganic solar cells. Chinese Physics B, 2022, 31, 038803.	1.4	2
11	Largeâ€Area and Efficient Skyâ€Blue Perovskite Lightâ€Emitting Diodes via Blade oating. Advanced Materials, 2022, 34, e2108939.	21.0	20
12	Step-by-Step Mechanism Insights into the TiO ₂ /Ce ₂ S ₃ S-Scheme Photocatalyst for Enhanced Aniline Production with Water as a Proton Source. ACS Catalysis, 2022, 12, 164-172.	11.2	117
13	Chemical insight into the hydrothermal deposition of Sb ₂ (S,Se) ₃ towards delicate microstructure engineering. Journal of Materials Chemistry A, 2022, 10, 9892-9901.	10.3	16
14	Heteroepitaxial and homoepitaxial nucleation strategies to grow Sb2S3 nanorod arrays and therefrom a derived gain of 7.18%-efficient Sb2(S,Se)3 quasi-nanoarray heterojunction solar cells. Applied Materials Today, 2022, 27, 101487.	4.3	13
15	A Transparent, Highâ€Performance, and Stable Sb ₂ S ₃ Photoanode Enabled by Heterojunction Engineering with Conjugated Polycarbazole Frameworks for Unbiased Photoelectrochemical Overall Water Splitting Devices. Advanced Materials, 2022, 34, e2200723.	21.0	30
16	Support Amorphization Engineering Regulates Single-Atom Ru as an Electron Pump for Nitrogen Photofixation. ACS Catalysis, 2022, 12, 8139-8146.	11.2	20
17	Dual effect of NH4F additive in the hydrothermal deposition of antimony selenosulfide thin film for high-performance solar cells. Science China Materials, 2022, 65, 3411-3417.	6.3	11
18	An Improbable Aminoâ€Functionalized Fullerene Spacer Enables 2D/3D Hybrid Perovskite with Enhanced Electron Transport in Solar Cells. Advanced Functional Materials, 2022, 32, .	14.9	11

#	Article	IF	CITATIONS
19	Post-Treatment of TiO ₂ Film Enables High-Quality Sb ₂ Se ₃ Film Deposition for Solar Cell Applications. ACS Applied Materials & Interfaces, 2022, 14, 33181-33190.	8.0	16
20	9.7%-efficient Sb ₂ (S,Se) ₃ solar cells with a dithieno[3,2- <i>b</i> : 2′,3′- <i>d</i>]pyrrole-cored hole transporting material. Energy and Environmental Science, 2021, 14, 359-364.	30.8	70
21	Photophysical characteristics and photosensitizing abilities of thieno[3,2-b]thiophene-Based photosensitizers for photovoltaic and photocatalytic applications. Journal of Photochemistry and Photobiology A: Chemistry, 2021, 406, 112979.	3.9	6
22	Defectâ€Resolved Effective Majority Carrier Mobility in Highly Anisotropic Antimony Chalcogenide Thinâ€Film Solar Cells. Solar Rrl, 2021, 5, 2000693.	5.8	22
23	Efficient Sb ₂ (S,Se) ₃ Solar Modules Enabled by Hydrothermal Deposition. Solar Rrl, 2021, 5, 2000750.	5.8	11
24	Synthesis of Janus Au@BCP nanoparticles <i>via</i> UV light-initiated RAFT polymerization-induced self-assembly. Nanoscale Advances, 2021, 3, 347-352.	4.6	9
25	Sequential Coevaporation and Deposition of Antimony Selenosulfide Thin Film for Efficient Solar Cells. Advanced Materials, 2021, 33, e2006689.	21.0	33
26	Direct Hydrothermal Deposition of Antimony Triselenide Films for Efficient Planar Heterojunction Solar Cells. ACS Applied Materials & Interfaces, 2021, 13, 18856-18864.	8.0	48
27	Heterometallic Seedâ€Mediated Zinc Deposition on Inkjet Printed Silver Nanoparticles Toward Foldable and Heatâ€Resistant Zinc Batteries. Advanced Functional Materials, 2021, 31, 2101607.	14.9	109
28	Revealing composition and structure dependent deep-level defect in antimony trisulfide photovoltaics. Nature Communications, 2021, 12, 3260.	12.8	113
29	Deep‣evel Transient Spectroscopy for Effective Passivator Selection in Perovskite Solar Cells to Attain High Efficiency over 23%. ChemSusChem, 2021, 14, 3182-3189.	6.8	24
30	Dendrite-Free Anodes Enabled by a Composite of a ZnAl Alloy with a Copper Mesh for High-Performing Aqueous Zinc-Ion Batteries. ACS Applied Materials & Interfaces, 2021, 13, 28129-28139.	8.0	47
31	Engineering microstructures for efficient Sb ₂ (S _x Se _{1â^`x) Tj ETQq1 1 0.784314}	rg <u>BT</u> /Ove	erloçk 10 Tf 5 4
32	Nanoarray heterojunction and its efficient solar cells without negative impact of photogenerated electric field. Communications Physics, 2021, 4, .	5.3	11
33	Solutionâ€Processed Compact Sb ₂ S ₃ Thin Films by a Facile One‣tep Deposition Method for Efficient Solar Cells. Solar Rrl, 2021, 5, 2100666.	5.8	16
34	CsPbBr ₃ Nanocrystal Induced Bilateral Interface Modification for Efficient Planar Perovskite Solar Cells. Advanced Science, 2021, 8, e2102648.	11.2	92
35	Efficient coaxial n-i-p heterojunction Sb ₂ S ₃ solar cells. Journal Physics D: Applied Physics, 2021, 54, 134001.	2.8	12
36	Solution processed AgSbS2 film for efficient planar heterojunction solar cells. Applied Physics Letters, 2021, 119, .	3.3	13

#	Article	IF	CITATIONS
37	Gold atom diffusion assisted thermal healing enabling high-performance hole-transporting material in solar cells. Applied Physics Letters, 2021, 119, .	3.3	4
38	Bulk heterojunction gifts bismuth-based lead-free perovskite solar cells with record efficiency. Nano Energy, 2020, 68, 104362.	16.0	102
39	Perovskite Quantum Dots Exhibiting Strong Hole Extraction Capability for Efficient Inorganic Thin Film Solar Cells. Cell Reports Physical Science, 2020, 1, 100001.	5.6	28
40	Probing the trap states in N–i–P Sb2(S,Se)3 solar cells by deep-level transient spectroscopy. Journal of Chemical Physics, 2020, 153, 124703.	3.0	16
41	Hydrothermal deposition of antimony selenosulfide thin films enables solar cells with 10% efficiency. Nature Energy, 2020, 5, 587-595.	39.5	338
42	Aqueous solution processed MoS ₃ as an eco-friendly hole-transport layer for all-inorganic Sb ₂ Se ₃ solar cells. Chemical Communications, 2020, 56, 15173-15176.	4.1	10
43	Manipulating the Electrical Properties of Sb ₂ (S,Se) ₃ Film for Highâ€Efficiency Solar Cell. Advanced Energy Materials, 2020, 10, 2002341.	19.5	137
44	Sb ₂ S ₃ Seed-Mediated Growth of Low-Defect Sb ₂ S ₃ on a TiO ₂ Substrate for Efficient Solar Cells. ACS Applied Energy Materials, 2020, 3, 12417-12422.	5.1	26
45	Macroscopic Orientational Gold Nanorods Monolayer Film with Excellent Photothermal Anticounterfeiting Performance. Advanced Optical Materials, 2020, 8, 1902082.	7.3	33
46	Controllable growth and flexible optoelectronic devices of regularly-assembled Bi2S3 semiconductor nanowire bifurcated junctions and crosslinked networks. Nano Research, 2020, 13, 2226-2232.	10.4	16
47	Efficient defect passivation of Sb ₂ Se ₃ film by tellurium doping for high performance solar cells. Journal of Materials Chemistry A, 2020, 8, 6510-6516.	10.3	48
48	Water Additive Enhanced Solution Processing of Alloy Sb ₂ (S _{1â^'<i>x</i>} Se _{<i>x</i>}) ₃ â€Based Solar Cells. Solar Rrl, 2020, 4, 1900582.	5.8	38
49	All Antimony Chalcogenide Tandem Solar Cell. Solar Rrl, 2020, 4, 2000048.	5.8	38
50	Pulsed laser deposition of antimony selenosulfide thin film for efficient solar cells. Applied Physics Letters, 2020, 116, .	3.3	16
51	Tunable Mie Resonances of Tin-based Iodide Perovskite Islandlike Films with Enhanced Infrared Photoluminescence. Journal of Physical Chemistry Letters, 2020, 11, 3332-3338.	4.6	8
52	Dendrite-Free and Stable Lithium Metal Anodes Enabled by an Antimony-Based Lithiophilic Interphase. Chemistry of Materials, 2019, 31, 7565-7573.	6.7	73
53	Chelation-assisted formation of multi-yolk–shell Co ₄ N@carbon nanoboxes for self-discharge-suppressed high-performance Li–SeS ₂ batteries. Journal of Materials Chemistry A, 2019, 7, 20302-20309.	10.3	29
54	Ultrafast self-trapping of photoexcited carriers sets the upper limit on antimony trisulfide photovoltaic devices. Nature Communications, 2019, 10, 4540.	12.8	117

#	Article	IF	CITATIONS
55	Nitrogenâ€Doped Nickel Oxide as Hole Transport Layer for Highâ€Efficiency Inverted Planar Perovskite Solar Cells. Solar Rrl, 2019, 3, 1900164.	5.8	29
56	Solution-Processed in Situ Growth of CuInS ₂ Nanoparticle Films for Efficient Planar Heterojunction Solar Cells with a Dual Nature of Charge Generation. ACS Applied Energy Materials, 2019, 2, 5231-5242.	5.1	29
57	Intermetallic SnSb nanodots embedded in carbon nanotubes reinforced nanofabric electrodes with high reversibility and rate capability for flexible Li-ion batteries. Nanoscale, 2019, 11, 13282-13288.	5.6	27
58	All-polymer particulate slurry batteries. Nature Communications, 2019, 10, 2513.	12.8	91
59	van der Waals Epitaxial Growth and Interfacial Passivation of Two-Dimensional Single-Crystalline Few-Layer Gray Arsenic Nanoflakes. Chemistry of Materials, 2019, 31, 4524-4535.	6.7	41
60	High-performance Li-ion capacitor based on black-TiO2-x/graphene aerogel anode and biomass-derived microporous carbon cathode. Nano Research, 2019, 12, 1713-1719.	10.4	64
61	Oscillator strengths and integral cross sections of the ÃA2″1↕X̃1A1excitation of ammonia studied by fast electron impact. Journal of Chemical Physics, 2019, 150, 064311.	3.0	5
62	Lowâ€Temperature In Situ Amino Functionalization of TiO ₂ Nanoparticles Sharpens Electron Management Achieving over 21% Efficient Planar Perovskite Solar Cells. Advanced Materials, 2019, 31, e1806095.	21.0	194
63	Composition engineering of Sb2S3 film enabling high performance solar cells. Science Bulletin, 2019, 64, 136-141.	9.0	41
64	Over 6% Certified Sb ₂ (S,Se) ₃ Solar Cells Fabricated via In Situ Hydrothermal Growth and Postselenization. Advanced Electronic Materials, 2019, 5, 1800683.	5.1	78
65	A thiol-amine mixture for metal oxide towards device quality metal chalcogenides. Science China Materials, 2019, 62, 899-906.	6.3	10
66	Interfacial Engineering by Indium-Doped CdS for High Efficiency Solution Processed Sb ₂ (S _{1–<i>x</i>} Se _{<i>x</i>}) ₃ Solar Cells. ACS Applied Materials & Interfaces, 2019, 11, 3207-3213.	8.0	59
67	Alkali Metals Doping for Highâ€Performance Planar Heterojunction Sb ₂ S ₃ Solar Cells. Solar Rrl, 2019, 3, 1800272.	5.8	94
68	Interfacial engineering for high efficiency solution processed Sb2Se3 solar cells. Solar Energy Materials and Solar Cells, 2019, 189, 5-10.	6.2	85
69	Coaxial MnO ₂ Nanoshell/CNFs Composite Film Anode for High-Performance Lithium-Ion Batteries. Journal of the Electrochemical Society, 2018, 165, A487-A492.	2.9	12
70	<i>β</i> â€Functionalized Imidazoleâ€Fused Porphyrinâ€Donorâ€Based Dyes: Effect of Ï€â€Linker and Acceptor Optoelectronic and Photovoltaic Properties. ChemistrySelect, 2018, 3, 2558-2564.	on 1.5	11
71	Direct solution deposition of device quality Sb2S3-xSex films for high efficiency solar cells. Solar Energy Materials and Solar Cells, 2018, 183, 52-58.	6.2	72
72	Strong Capillarity, Chemisorption, and Electrocatalytic Capability of Crisscrossed Nanostraws Enabled Flexible, High-Rate, and Long-Cycling Lithium–Sulfur Batteries. ACS Nano, 2018, 12, 4868-4876.	14.6	222

#	Article	IF	CITATIONS
73	Phosphotungstic Acid Regulated Chemical Bath Deposition of Sb ₂ S ₃ for Highâ€Efficiency Planar Heterojunction Solar Cell. Energy Technology, 2018, 6, 2126-2131.	3.8	18
74	Oscillator strengths and integral cross sections for the valence-shell excitations of nitric oxide studied by fast electron impact. Journal of Chemical Physics, 2018, 148, 044311.	3.0	9
75	Interface Engineering of Anchored Ultrathin TiO ₂ /MoS ₂ Heterolayers for Highly-Efficient Electrochemical Hydrogen Production. ACS Applied Materials & Interfaces, 2018, 10, 6084-6089.	8.0	47
76	Phase Engineering of Perovskite Materials for High-Efficiency Solar Cells: Rapid Conversion of CH ₃ NH ₃ PbI ₃ to Phase-Pure CH ₃ NH ₃ PbCl ₃ via Hydrochloric Acid Vapor Annealing Post-Treatment, ACS Applied Materials & amp; Interfaces, 2018, 10, 1897-1908.	8.0	62
77	Walnutâ€Like Multicore–Shell MnO Encapsulated Nitrogenâ€Rich Carbon Nanocapsules as Anode Material for Longâ€Cycling and Softâ€Packed Lithiumâ€Ion Batteries. Advanced Functional Materials, 2018, 28, 1800003.	14.9	191
78	Development of antimony sulfide–selenide Sb2(S, Se)3-based solar cells. Journal of Energy Chemistry, 2018, 27, 713-721.	12.9	166
79	Integrated perovskite solar capacitors with high energy conversion efficiency and fast photo-charging rate. Journal of Materials Chemistry A, 2018, 6, 2047-2052.	10.3	85
80	Sequential deposition route to efficient Sb ₂ S ₃ solar cells. Journal of Materials Chemistry A, 2018, 6, 21320-21326.	10.3	46
81	Atomic Substitution Enabled Synthesis of Vacancy-Rich Two-Dimensional Black TiO _{2–<i>x</i>} Nanoflakes for High-Performance Rechargeable Magnesium Batteries. ACS Nano, 2018, 12, 12492-12502.	14.6	116
82	Efficient Perovskite Solar Cells with Titanium Cathode Interlayer (Solar RRL 11â^•2018). Solar Rrl, 2018, 2, 1870226.	5.8	1
83	Solution Processed Antimony Sulfide-Selenide [Sb <inf>2</inf> (S,Se) <inf>3</inf>] for High Efficiency Solar Cells. , 2018, , .		1
84	Promising Sb ₂ (S,Se) ₃ Solar Cells with High Open Voltage by Application of a TiO ₂ /CdS Double Buffer Layer. Solar Rrl, 2018, 2, 1800208.	5.8	83
85	Solution processed NiOx hole-transporting material for all-inorganic planar heterojunction Sb2S3 solar cells. Solar Energy Materials and Solar Cells, 2018, 185, 542-548.	6.2	50
86	Highly Branched VS ₄ Nanodendrites with 1D Atomic hain Structure as a Promising Cathode Material for Longâ€Cycling Magnesium Batteries. Advanced Materials, 2018, 30, e1802563.	21.0	187
87	V ₂ O ₅ as Hole Transporting Material for Efficient All Inorganic Sb ₂ S ₃ Solar Cells. ACS Applied Materials & Interfaces, 2018, 10, 27098-27105.	8.0	88
88	Aqueousâ€Solutionâ€Based Approach Towards Carbonâ€Free Sb ₂ S ₃ Films for High Efficiency Solar Cells. ChemSusChem, 2018, 11, 3208-3214.	6.8	15
89	Vacuum assisted solution processing for highly efficient Sb ₂ S ₃ solar cells. Journal of Materials Chemistry A, 2018, 6, 16322-16327.	10.3	53
90	Investigations of the valence-shell excitations of molecular ethane by high-energy electron scattering. Journal of Chemical Physics, 2018, 148, 144313.	3.0	2

#	Article	IF	CITATIONS
91	Three-dimensional spongy framework as superlyophilic, strongly absorbing, and electrocatalytic polysulfide reservoir layer for high-rate and long-cycling lithium-sulfur batteries. Nano Research, 2018, 11, 6436-6446.	10.4	38
92	Efficient Perovskite Solar Cells with Titanium Cathode Interlayer. Solar Rrl, 2018, 2, 1800167.	5.8	16
93	n-Type Doping of Sb ₂ S ₃ Light-Harvesting Films Enabling High-Efficiency Planar Heterojunction Solar Cells. ACS Applied Materials & Interfaces, 2018, 10, 30314-30321.	8.0	103
94	Solution Processed Sb2(S, Se)3 Solar Cells. , 2018, , .		0
95	Bottom-up synthesis of nitrogen-doped porous carbon scaffolds for lithium and sodium storage. Nanoscale, 2017, 9, 1972-1977.	5.6	42
96	A fast chemical approach towards Sb ₂ S ₃ film with a large grain size for high-performance planar heterojunction solar cells. Nanoscale, 2017, 9, 3386-3390.	5.6	145
97	Bis(phenothiazylâ€ethynylene)â€Based Organic Dyes Containing Diâ€Anchoring Groups with Efficiency Comparable to N719 for Dyeâ€5ensitized Solar Cells. Chemistry - an Asian Journal, 2017, 12, 332-340.	3.3	9
98	Seleniumâ€Graded Sb ₂ (S _{1â^'x} Se _x) ₃ for Planar Heterojunction Solar Cell Delivering a Certified Power Conversion Efficiency of 5.71%. Solar Rrl, 2017, 1, 1700017.	5.8	82
99	Controlled growth and photoconductive properties of hexagonal SnS2 nanoflakes with mesa-shaped atomic steps. Nano Research, 2017, 10, 1434-1447.	10.4	51
100	Highly Efficient Retention of Polysulfides in "Sea Urchin―Like Carbon Nanotube/Nanopolyhedra Superstructures as Cathode Material for Ultralong-Life Lithium–Sulfur Batteries. Nano Letters, 2017, 17, 437-444.	9.1	223
101	Pine needle-derived microporous nitrogen-doped carbon frameworks exhibit high performances in electrocatalytic hydrogen evolution reaction and supercapacitors. Nanoscale, 2017, 9, 1237-1243.	5.6	154
102	Successive surface engineering of TiO ₂ compact layers via dual modification of fullerene derivatives affording hysteresis-suppressed high-performance perovskite solar cells. Journal of Materials Chemistry A, 2017, 5, 1724-1733.	10.3	77
103	Self-Templated Formation of Interlaced Carbon Nanotubes Threaded Hollow Co ₃ S ₄ Nanoboxes for High-Rate and Heat-Resistant Lithium–Sulfur Batteries. Journal of the American Chemical Society, 2017, 139, 12710-12715.	13.7	456
104	Cu _{2â°'x} GeS ₃ : a new hole transporting material for stable and efficient perovskite solar cells. Journal of Materials Chemistry A, 2017, 5, 19884-19891.	10.3	17
105	Nonconjugated Polymer Poly(vinylpyrrolidone) as an Efficient Interlayer Promoting Electron Transport for Perovskite Solar Cells. ACS Applied Materials & Interfaces, 2017, 9, 32957-32964.	8.0	73
106	Porous-Shell Vanadium Nitride Nanobubbles with Ultrahigh Areal Sulfur Loading for High-Capacity and Long-Life Lithium–Sulfur Batteries. Nano Letters, 2017, 17, 7839-7846.	9.1	206
107	Cerium Oxide Nanocrystal Embedded Bimodal Micromesoporous Nitrogen-Rich Carbon Nanospheres as Effective Sulfur Host for Lithium–Sulfur Batteries. ACS Nano, 2017, 11, 7274-7283.	14.6	213
108	MoS ₂ â€Based Allâ€Purpose Fibrous Electrode and Selfâ€Powering Energy Fiber for Efficient Energy Harvesting and Storage. Advanced Energy Materials, 2017, 7, 1601208.	19.5	139

#	Article	IF	CITATIONS
109	Synthesis and Characterization of Phenothiazineâ€Based Platinum(II)–Acetylide Photosensitizers for Efficient Dyeâ€Sensitized Solar Cells. Chemistry - A European Journal, 2016, 22, 3750-3757.	3.3	27
110	Photostability and Moisture Stability of CH ₃ NH ₃ PbI ₃ â€based Solar Cells by Ethyl Cellulose. ChemPlusChem, 2016, 81, 1292-1298.	2.8	23
111	Pitaya-like microspheres derived from Prussian blue analogues as ultralong-life anodes for lithium storage. Journal of Materials Chemistry A, 2016, 4, 15041-15048.	10.3	35
112	Hierarchical Ternary Carbide Nanoparticle/Carbon Nanotube-Inserted N-Doped Carbon Concave-Polyhedrons for Efficient Lithium and Sodium Storage. ACS Applied Materials & Interfaces, 2016, 8, 26834-26841.	8.0	52
113	Hierarchical porous nitrogen-rich carbon nanospheres with high and durable capabilities for lithium and sodium storage. Nanoscale, 2016, 8, 17911-17918.	5.6	57
114	Exceptionally Stable CH ₃ NH ₃ PbI ₃ Films in Moderate Humid Environmental Condition. Advanced Science, 2016, 3, 1500262.	11.2	50
115	All-Inorganic Perovskite Solar Cells. Journal of the American Chemical Society, 2016, 138, 15829-15832.	13.7	899
116	Solution-Processable Ionic Liquid as an Independent or Modifying Electron Transport Layer for High-Efficiency Perovskite Solar Cells. ACS Applied Materials & Interfaces, 2016, 8, 34464-34473.	8.0	111
117	In Situ Thermal Synthesis of Inlaid Ultrathin MoS ₂ /Graphene Nanosheets as Electrocatalysts for the Hydrogen Evolution Reaction. Chemistry of Materials, 2016, 28, 5733-5742.	6.7	166
118	Investigation on a dopant-free hole transport material for perovskite solar cells. RSC Advances, 2016, 6, 69365-69369.	3.6	25
119	Acetate Salts as Nonhalogen Additives To Improve Perovskite Film Morphology for High-Efficiency Solar Cells. ACS Applied Materials & Interfaces, 2016, 8, 15333-15340.	8.0	56
120	Crystallinity and defect state engineering in organo-lead halide perovskite for high-efficiency solar cells. Journal of Materials Chemistry A, 2016, 4, 3806-3812.	10.3	76
121	Li ₃ V ₂ (PO ₄) ₃ encapsulated flexible free-standing nanofabric cathodes for fast charging and long life-cycle lithium-ion batteries. Nanoscale, 2016, 8, 7408-7415.	5.6	49
122	Molecular engineering of starburst triarylamine donor with selenophene containing π-linker for dye-sensitized solar cells. Journal of Materials Chemistry C, 2016, 4, 713-726.	5.5	23
123	Synthesis of tunable-band-gap "Open-Box―halide perovskites by use of anion exchange and internal dissolution procedures. Journal of Colloid and Interface Science, 2016, 461, 162-167.	9.4	2
124	Co-sensitization of 3D bulky phenothiazine-cored photosensitizers with planar squaraine dyes for efficient dye-sensitized solar cells. Journal of Materials Chemistry A, 2015, 3, 13848-13855.	10.3	52
125	Elucidating the Reaction Pathways in the Synthesis of Organolead Trihalide Perovskite for High-Performance Solar Cells. Scientific Reports, 2015, 5, 10557.	3.3	48
126	Ruthenium-Based Photosensitizers for Dye-Sensitized Solar Cells. Green Chemistry and Sustainable Technology, 2015, , 91-114.	0.7	9

#	Article	IF	CITATIONS
127	Light-Triggered Reversible Self-Assembly of Gold Nanoparticle Oligomers for Tunable SERS. Langmuir, 2015, 31, 1164-1171.	3.5	101
128	Novel D-Ï€-A organic sensitizers containing diarylmethylene-bridged triphenylamine and different spacers for solar cell application. Tetrahedron Letters, 2015, 56, 1233-1238.	1.4	24
129	SnS ₂ nanosheet-based microstructures with high adsorption capabilities and visible light photocatalytic activities. RSC Advances, 2015, 5, 24640-24648.	3.6	66
130	Additive regulated crystallization and film formation of CH ₃ NH ₃ PbI _{3â^x} Br _x for highly efficient planar-heterojunction solar cells. Journal of Materials Chemistry A, 2015, 3, 18514-18520.	10.3	49
131	Novel organic dyes based on diarylmethylene-bridged triphenylamine for dye-sensitized solar cells. Synthetic Metals, 2015, 205, 70-77.	3.9	26
132	Dye-sensitized solar cells based on functionalized truxene structure. Chinese Chemical Letters, 2015, 26, 955-962.	9.0	3
133	Engineering hollow mesoporous silica nanocontainers with molecular switches for continuous self-healing anticorrosion coating. Journal of Materials Chemistry A, 2015, 3, 9510-9516.	10.3	89
134	New Organic Dyes Based on Biarylmethyleneâ€Bridged Triphenylamine for Dye Sensitized Solar Cell. Chinese Journal of Chemistry, 2015, 33, 925-933.	4.9	5
135	Template Synthesis of CuInS ₂ Nanocrystals from In ₂ S ₃ Nanoplates and Their Application as Counter Electrodes in Dye-Sensitized Solar Cells. Chemistry of Materials, 2015, 27, 5949-5956.	6.7	132
136	Effects of various π-conjugated spacers in thiadiazole[3,4-c]pyridine-cored panchromatic organic dyes for dye-sensitized solar cells. Journal of Materials Chemistry A, 2015, 3, 3103-3112.	10.3	41
137	Hybrid ZnO Nanorodâ€Polymer Brush Hierarchically Nanostructured Substrate for Sensitive Antibody Microarrays. Advanced Materials, 2015, 27, 181-185.	21.0	67
138	Linear or quadratic plasmon peak sensitivities for individual Au/Ag nanosphere sensors. Sensors and Actuators B: Chemical, 2014, 203, 812-816.	7.8	9
139	Molecular Engineering of Simple Phenothiazineâ€Based Dyes To Modulate Dye Aggregation, Charge Recombination, and Dye Regeneration in Highly Efficient Dyeâ€Sensitized Solar Cells. Chemistry - A European Journal, 2014, 20, 6300-6308.	3.3	88
140	Effective improvement of the photovoltaic performance of black dye sensitized quasi-solid-state solar cells. RSC Advances, 2014, 4, 31759-31763.	3.6	11
141	Fluorene-bridged organic dyes with di-anchoring groups for efficient co-adsorbent-free dye-sensitized solar cells. Journal of Materials Chemistry C, 2014, 2, 7086.	5.5	33
142	Graphene oxide-enabled tandem signal amplification for sensitive SPRi immunoassay in serum. Chemical Communications, 2014, 50, 2133.	4.1	45
143	Panchromatic light harvesting by N719 with a porphyrin molecule for high-performance dye-sensitized solar cells. Journal of Materials Chemistry C, 2014, 2, 3521.	5.5	26
144	(Gold core)/(titania shell) nanostructures for plasmon-enhanced photon harvesting and generation of reactive oxygen species. Energy and Environmental Science, 2014, 7, 3431-3438.	30.8	180

#	Article	IF	CITATIONS
145	Perovskite photovoltaics: a high-efficiency newcomer to the solar cell family. Nanoscale, 2014, 6, 12287-12297.	5.6	120
146	Optimizing the photovoltaic performance of thiocyanate-free ruthenium photosensitizers by structural modification of C^N cyclometalating ligand in dye-sensitized solar cells. Polyhedron, 2014, 82, 71-79.	2.2	9
147	Printable Highly Catalytic Pt- and TCO-Free Counter Electrode for Dye-Sensitized Solar Cells. ACS Applied Materials & Interfaces, 2014, 6, 2224-2229.	8.0	32
148	Few-Layer MoSe2 Possessing High Catalytic Activity towards Iodide/Tri-iodide Redox Shuttles. Scientific Reports, 2014, 4, 4063.	3.3	70
149	Conformational engineering of co-sensitizers to retard back charge transfer for high-efficiency dye-sensitized solar cells. Journal of Materials Chemistry A, 2013, 1, 11553.	10.3	94
150	Improving Pore Filling of Gel Electrolyte and Charge Transport in Photoanode for High-Efficiency Quasi-Solid-State Dye-Sensitized Solar Cells. ACS Applied Materials & Interfaces, 2013, 5, 8289-8293.	8.0	15
151	Dielectric Nanocup Coating Effect on the Resonant Optical Properties of Individual Au Nanosphere. Plasmonics, 2013, 8, 1523-1527.	3.4	6
152	Thiocyanate-free ruthenium(II) cyclometalated complexes containing uncommon thiazole and benzothiazole chromophores for dye-sensitized solar cells. Journal of Organometallic Chemistry, 2013, 748, 75-83.	1.8	25
153	New phenothiazine-based dyes for efficient dye-sensitized solar cells: Positioning effect of a donor group on the cell performance. Journal of Power Sources, 2013, 243, 253-259.	7.8	74
154	A portable flow-through fluorescent immunoassay lab-on-a-chip device using ZnO nanorod-decorated glass capillaries. Lab on A Chip, 2013, 13, 1797.	6.0	47
155	Significant Improvement of Dye-Sensitized Solar Cell Performance Using Simple Phenothiazine-Based Dyes. Chemistry of Materials, 2013, 25, 2146-2153.	6.7	250
156	Interface Functionalization of Photoelectrodes with Graphene for High Performance Dye ensitized Solar Cells. Advanced Functional Materials, 2012, 22, 5245-5250.	14.9	135
157	Enhancement of low energy sunlight harvesting in dye-sensitized solar cells using plasmonic gold nanorods. Energy and Environmental Science, 2012, 5, 9444.	30.8	203
158	Thermoelectric Bi ₂ Te ₃ -improved charge collection for high-performance dye-sensitized solar cells. Energy and Environmental Science, 2012, 5, 6294-6298.	30.8	77
159	Engineering "Hot―Nanoparticles for Surfaceâ€Enhanced Raman Scattering by Embedding Reporter Molecules in Metal Layers. Small, 2012, 8, 246-251.	10.0	128
160	Efficient iodine-free dye-sensitized solar cells employing truxene-based organic dyes. Chemical Communications, 2012, 48, 6645.	4.1	47
161	Surfaceâ€enhanced Raman scattering on silver dendrite with different growth directions. Journal of Raman Spectroscopy, 2012, 43, 396-404.	2.5	12
162	QSAR prediction of HIV inhibition activity of styrylquinoline derivatives by genetic algorithm coupled with multiple linear regressions. Medicinal Chemistry Research, 2012, 21, 437-443.	2.4	19

#	Article	IF	CITATIONS
163	Graphene- <mml:math <br="" altimg="si1.gif" xmlns:mml="http://www.w3.org/1998/Math/MathML">overflow="scroll"><mml:mrow><mml:mtext>Pt</mml:mtext><mml:mo>â§1</mml:mo><mml:mtext>ITOcounter electrode to significantly reduce Pt loading and enhance charge transfer for high performance dye-sensitized solar cell. Solar Energy, 2012, 86, 2041-2048.</mml:mtext></mml:mrow></mml:math>	ntext> 6.1	ıml;mrow>
164	Multivariate Calibration of Near Infrared Spectroscopy in the Presence of Light Scattering Effect: A Comparative Study. Analytical Letters, 2011, 44, 824-836.	1.8	24
165	Site-selective localization of analytes on gold nanorod surface for investigating field enhancement distribution in surface-enhanced Raman scattering. Nanoscale, 2011, 3, 1575.	5.6	39
166	Hydrogen storage in Ni–B nanoalloy-doped 2D graphene. International Journal of Hydrogen Energy, 2011, 36, 12950-12954.	7.1	47
167	Surface functionalization-enhanced spillover effect on hydrogen storage of Ni–B nanoalloy-doped activated carbon. International Journal of Hydrogen Energy, 2011, 36, 13663-13668.	7.1	42
168	A Hierarchically Nanostructured Composite of MnO ₂ /Conjugated Polymer/Graphene for Highâ€Performance Lithium Ion Batteries. Advanced Energy Materials, 2011, 1, 736-741.	19.5	279
169	Probing the Kinetics of Shortâ€Ðistance Drug Release from Nanocarriers to Nanoacceptors. Angewandte Chemie - International Edition, 2010, 49, 8426-8430.	13.8	39
170	Rational control of anisotropic nanocomposites for engineered nanocatives and SERS application. , 2010, , .		1
171	Reducing the Symmetry of Bimetallic Au@Ag Nanoparticles by Exploiting Eccentric Polymer Shells. Journal of the American Chemical Society, 2010, 132, 9537-9539.	13.7	121
172	Hotspot-Induced Transformation of Surface-Enhanced Raman Scattering Fingerprints. ACS Nano, 2010, 4, 3087-3094.	14.6	203
173	Scalable Routes to Janus Auâ^'SiO ₂ and Ternary Agâ^'Auâ^'SiO ₂ Nanoparticles. Chemistry of Materials, 2010, 22, 3826-3828.	6.7	168
174	Mechanical Nanosprings: Induced Coiling and Uncoiling of Ultrathin Au Nanowires. Journal of the American Chemical Society, 2010, 132, 11920-11922.	13.7	99
175	Development of Polymerâ€Encapsulated Metal Nanoparticles as Surfaceâ€Enhanced Raman Scattering Probes. Small, 2009, 5, 198-202.	10.0	145
176	Microcanonical analysis of adsorption of homopolymer chain on a surface. Journal of Chemical Physics, 2009, 130, 244905.	3.0	12
177	Bayesian linear regression and variable selection for spectroscopic calibration. Analytica Chimica Acta, 2009, 631, 13-21.	5.4	69
178	Statistical Modelling and Analysis of the Aerobic Oxidation of Benzyl Alcohol over K–Mn/C Catalysts. Catalysis Letters, 2009, 128, 210-220.	2.6	18
179	Application of the simple model for f–d transition to assignment of 4f–5d excitation spectra of Yb ³⁺ doped in crystals. Physica Status Solidi (B): Basic Research, 2009, 246, 1050-1055.	1.5	1
180	Fabrication of Polymer Nanocavities with Tailored Openings. ACS Nano, 2009, 3, 3469-3474.	14.6	88

#	Article	IF	CITATIONS
181	Facile fabrication of triple-layer (Au@Ag)@polypyrrole core–shell and (Au@H2O)@polypyrrole yolk–shell nanostructures. Chemical Communications, 2009, , 1653.	4.1	70
182	Polymer-Encapsulated Gold-Nanoparticle Dimers: Facile Preparation and Catalytical Application in Guided Growth of Dimeric ZnO-Nanowires. Nano Letters, 2008, 8, 2643-2647.	9.1	155
183	Controlled Assembly of Eccentrically Encapsulated Gold Nanoparticles. Journal of the American Chemical Society, 2008, 130, 11858-11859.	13.7	201
184	Elastic Behavior of Polymer Chains. Chinese Journal of Chemical Physics, 2008, 21, 463-468.	1.3	1
185	Factors Affecting Polymer Translocation Through a Nanopore in a Membrane. Chinese Journal of Chemical Physics, 2008, 21, 275-280.	1.3	2
186	Microcanonical analyses of homopolymer aggregation processes. Physical Review E, 2008, 78, 056101.	2.1	12
187	Intrinsic Trapping and Recombination Dynamics in Lowâ€Dimensional Bismuth Sulfide Nanocrystals. Advanced Materials Interfaces, 0, , 2200219.	3.7	1